Plasma dynamics at the Schwinger limit and beyond

Gert Brodin,[1,*] Haidar Al-Naseri [1,†] Jens Zamanian,[1] Greger Torgrimsson,[1] and Bengt Eliasson [2]

[1]*Department of Physics, Umeå University, SE-901 87 Umeå, Sweden*
[2]*SUPA, Department of Physics, University of Strathclyde, Glasgow G4 0NG, United Kingdom*

Strong field physics close to or above the Schwinger limit are typically studied with vacuum as initial condition or by considering test particle dynamics. However, with a plasma present initially, quantum relativistic mechanisms such as Schwinger pair creation are complemented by classical plasma nonlinearities. In this work we use the Dirac-Heisenberg-Wigner formalism to study the interplay between classical and quantum mechanical mechanisms in the regime of ultrastrong electric fields. In particular, the effects of initial density and temperature on the plasma oscillation dynamics are determined. Finally, comparisons with competing mechanisms such as radiation reaction and Breit-Wheeler pair production are made.

I. INTRODUCTION

In recent years, much research has been devoted to strong field physics where various QED effects come into play; see, e.g., Refs. [1,2] for review articles. A key motivating factor has been the rapid evolution of laser intensities [1–3]. Nevertheless, in spite of the steady progress, peak electric fields for current lasers are still well below the critical field strength $E_{cr} = m^2 c^3 / e\hbar \approx 1.3 \times 10^{18}$ V/m [4–7]. It should be noted, however, that there are proposals trying to use plasma-based schemes in order to magnify present-day laser fields to reach the Schwinger limit [8]. Whether laboratory-created field strengths of this magnitude actually can be possible has been debated in the recent literature; see, e.g., Refs [9–11]. Specifically, field depleting cascade mechanisms have been put forward as a severe obstacle in Refs [9,10]. However, an opposing pinch mechanism, effectively focusing the field, has been identified in Ref. [11]

Research on ultrahigh intensities, i.e., close to or above the Schwinger limit, has been particularly concerned with Schwinger pair creation in vacuum [12–16]. Problems of study include, e.g., understanding the interplay between temporal and spatial variations of the fields [13–15], comparing different computational schemes [12,14], or optimizing the geometry of colliding laser pulses to maximize pair creation [16,17].

For sufficiently strong fields, large number of pairs are created, leading to plasma currents modifying the original

---

*gert.brodin@umu.se
†haidar.al-naseri@umu.se

fields, such that the back-reaction through Ampère's law is relevant [18–31]. Starting the dynamics with a Sauter pulse [32] or a constant initial electric field, the system will undergo plasma oscillations, with a plasma frequency proportional to the peak electric field.

In the present paper we intend to study how the dynamics is modified when a plasma of high density is present initially. In this case several new questions enter the picture. How does the dynamics depend on the plasma temperature and density? What is the interplay between classical plasma nonlinearities and those due to quantum relativistic effects? To what extent can pair creation be blocked if the low-energy states are already occupied?

Specifically, we will use the Dirac-Heisenberg-Wigner (DHW) formalism [33] in order to address the above questions numerically, generalizing results from the linear regime [34] and/or using prescribed fields [35] into the strong field self-consistent regime. After theoretical preliminaries are settled, including the issue of charge renormalization, we study plasma oscillations in an electron-ion plasma focusing on the homogeneous limit. It is worth noting that with a plasma present from the start, the energy density necessary for pair creation can equally well be stored in the plasma current. In this case the initial electric field is zero, but the plasma kinetic energy is converted into an electric field of sufficient magnitude.

No restrictions on the electric field amplitude will be made, and thus the dynamics will be studied also for field strengths well beyond the critical field. For a field strength of the order of the critical field or higher, the plasma oscillations increase their frequency due to the pair-creation process, at the same time as they are damped.

This paper is organized as follows: In Sec. II we briefly discuss the derivation of the DHW formalism and present a reduced system applicable for electrostatic fields. In Sec. III we present the calculations relevant to charge renormalization. Next, the numerical results are presented in Sec. IV. Here we show the scaling of the damping with the initial electric

field amplitude and with the plasma parameters, study issues related to Pauli blocking, and relate our findings to previous results starting from vacuum. Finally, we discuss potential competing mechanisms such as radiation reaction in Sec. V and nonlinear Breit-Wheeler in Sec. VI, and we draw the conclusions in Sec. VII.

II. THE DHW FORMALISM

The analysis will be based on the DHW formalism, first presented in Ref. [33]. This formalism is based on a Hartree-Fock (mean-field) approximation. For an approach developing a self-consistent kinetic formalism without using the mean-field approximation, see, e.g., Ref. [36]. As for the DHW formalism, we note that slightly different derivations have also been presented by Refs. [12,37,38]. Since the presentation given in previous works are fully satisfactory, we will not give details of the derivations here, just point out the main features:

(1) The derivations is based on a Gauge invariant Wigner transformation of the Dirac equation, producing a 4 by 4 Wigner matrix (due to the Dirac four spinors). The Wigner operator $\hat{W}(\mathbf{r}, \mathbf{p}, t)$, depending on the phase space variables $\mathbf{r}$ and $\mathbf{p}$, is given by

$$\hat{W}(\mathbf{r}, \mathbf{p}, t)$$

$$= -\frac{1}{2} \int d^3 z \exp\left(-i\mathbf{p} \cdot \mathbf{z} - ie \int_{-1/2}^{1/2} d\lambda \mathbf{z} \cdot \mathbf{A}(\mathbf{r} + \lambda\mathbf{z}, t)\right)$$

$$\times [\hat{\Psi}(\mathbf{r} + \mathbf{z}/2, t), \hat{\bar{\Psi}}(\mathbf{r} - \mathbf{z}/2)], \tag{1}$$

where $\hat{\Psi}$ represents the Dirac spinor field, $\hat{\bar{\Psi}}$ denotes the Hermitian conjugate, $\mathbf{z}$ is the 3D position variable integrated over all space, and $\mathbf{A}$ is the vector potential. Note that the Wilson-line factor has been used to ensure the gauge invariance. The Wigner function $W(\mathbf{r}, \mathbf{p}, t)$ is defined as the expectation value of the Wigner operator

$$W(\mathbf{r}, \mathbf{p}, t) = \text{Tr}\hat{\rho}\hat{W}(\mathbf{r}, \mathbf{p}, t) = \sum_i p_i \langle \Omega_i | \hat{W}(\mathbf{r}, \mathbf{p}, t) | \Omega_i \rangle, \tag{2}$$

where $\hat{\rho} = \sum_i p_i |\Omega_i\rangle\langle\Omega_i|$ is the state of the system, and the sum of the probabilities p_i is unity.

(2) In the derivation, the vacuum fluctuations are dropped in comparison with the electromagnetic mean field, which is a particularly accurate approximation for strong field problems [33].

(3) The 16 components of $W(\mathbf{r}, \mathbf{p}, t)$ can be split using various projections, to formulate the theory in a physically attractive way. We have used the standard split of Refs. [12,33], which divides $W(\mathbf{r}, \mathbf{p}, t)$ into phase space functions for quantities like mass, charge density, current density, spin, and magnetization; see Ref. [33] for the full details.

(4) Since the DHW functions couple to current and charge sources, the system is closed by Maxwell's equations; see, e.g., Ref. [33].

With the closed system in place, further simplifications can be made depending on the geometry of the electromagnetic field. For the case of a 1D electrostatic field [39] $\mathbf{E} = E(z, t)\hat{\mathbf{z}}$,

the full system (see Ref. [35]) can be reduced to

$$D_t \chi_1(z, \mathbf{p}, t) = 2\varepsilon_\perp(p_\perp)\chi_3(z, \mathbf{p}, t) - \frac{\partial \chi_4}{\partial z}(z, \mathbf{p}, t),$$

$$D_t \chi_2(z, \mathbf{p}, t) = -2p_z \chi_3(z, \mathbf{p}, t),$$

$$D_t \chi_3(z, \mathbf{p}, t) = -2\varepsilon_\perp(p_\perp)\chi_1(z, \mathbf{p}, t) + 2p_z \chi_2(z, \mathbf{p}, t),$$

$$D_t \chi_4(z, \mathbf{p}, t) = -\frac{\partial \chi_1}{\partial z}(z, \mathbf{p}, t) \tag{3}$$

together with Ampère's law

$$\frac{\partial E}{\partial t} = -\frac{e}{(2\pi)^3} \int \chi_1 d^3 p, \tag{4}$$

where $D_t = \partial/\partial t + eE \partial/\partial p_z$ and $\varepsilon_\perp = \sqrt{m^2 + p_\perp^2}$, and where $p_\perp$ is the perpendicular momentum. The variable χ_1 is the (phase space) current density j_z,

$$j_z = \frac{e}{(2\pi)^3} \int \chi_1 d^3 p, \tag{5}$$

χ_2 gives the mass density ρ_m,

$$\rho_m = \frac{m}{(2\pi)^3} \int \frac{\chi_2}{\varepsilon_\perp} d^3 p, \tag{6}$$

χ_3 gives the spin density, i.e., the angular momentum density $\mathbf{M}$ due to the spin is

$$\mathbf{M} = \frac{1}{(2\pi)^3} \int (\hat{\mathbf{z}} \times \mathbf{p}) \frac{\chi_3}{2\varepsilon_\perp} d^3 p, \tag{7}$$

and χ_4 gives the charge density ρ_c,

$$\rho_c = \frac{e}{(2\pi)^3} \int \chi_4 d^3 p. \tag{8}$$

Next, we rewrite the system Eq. (3) to simplify the numerical calculations. In this context it is important to note that χ_1 and χ_2 have nonzero vacuum contributions, associated with the expectation values of the free Dirac field operators (see, e.g., Ref. [33,40]), where the vacuum expressions are given by

$$\chi_{1vac} = -\frac{2p_z}{\varepsilon},$$

$$\chi_{2vac} = -\frac{2\varepsilon_\perp}{\varepsilon}. \tag{9}$$

Here $\varepsilon = \sqrt{m^2 + p^2}$, and we introduce new variables $\tilde{\chi}_i(z, \mathbf{p}, t)$ as the deviation from the vacuum state; i.e., we let

$$\tilde{\chi}_i(z, \mathbf{p}, t) = \chi_i(z, \mathbf{p}, t) - \chi_{ivac}(\mathbf{p}). \tag{10}$$

Note that $\tilde{\chi}_{3,4} = \chi_{3,4}$. Second, we switch to the canonical momentum. Using the Weyl gauge where the scalar potential is zero such that $E = -\partial A/\partial t$, the z component of the kinetic momentum is replaced by $q = p_z + eA$. With q as one of the independent variables, the operator D_t simplifies to $D_t = \partial/\partial t$. Our third modification is to switch to dimensionless variables. The normalized variables are given by $t_n = \omega_c t$, $q_n = q/mc$, $p_{n\perp} = p_\perp/mc$, $E_n = E/E_{cr}$, $A_n = eA/mc$, where $\omega_c = (mc^2/\hbar)$ is the Compton frequency, and we note that the DHW functions are already normalized. For notational convenience, we omit the index n in what follows. Finally, we

consider the homogeneous limit, making the variable $\tilde{\chi}_4 = 0$. The equations to be solved numerically now read

$$\frac{\partial \tilde{\chi}_1}{\partial t}(q, p_\perp, t) = 2\varepsilon_\perp \tilde{\chi}_3 + 2E\frac{\varepsilon_\perp^2}{\varepsilon^3},$$

$$\frac{\partial \tilde{\chi}_2}{\partial t}(q, p_\perp, t) = -2(q-A)\tilde{\chi}_3 - 2(q-A)E\frac{\varepsilon_\perp}{\varepsilon^3}, \quad (11)$$

$$\frac{\partial \tilde{\chi}_3}{\partial t}(q, p_\perp, t) = -2\varepsilon_\perp \tilde{\chi}_1 + 2(q-A)\tilde{\chi}_2$$

with Ampère's law

$$\frac{\partial E}{\partial t} = -\eta \int \chi_1 \, d^2 p, \quad (12)$$

where the dimensionless factor $\eta = \alpha/\pi \approx 2.322 \times 10^{-3}$. Note that due to cylindrical symmetry the azimuthal integration has already been carried out and hence $d^2 p = p_\perp \, dq \, dp_\perp$.

Before ending this section, let us briefly discuss what physics that is included in the coupled system of Eqs. (11) and (12). Due to the mean-field approximation, as expected, single-particle Larmor emission will not be contained in the model, nor will processes involving few particles such as Breit-Wheeler pair-production be covered. We can note that by dropping all quantum effects, the model reduces to the 1D electrostatic limit of the relativistic Vlasov equations. However, all quantum effects that can be described as a collective phenomenon are generally included in the model. Specifically this includes, e.g., collective pair creation, collective pair annihilation, Pauli blocking, and vacuum effects such as a finite vacuum polarization [34]. The vacuum contribution also give rise to the issue of charge renormalization, that will be discussed in the next section.

III. CHARGE RENORMALIZATION

Generally, the integrals in Ampère's law in Eq. (12) are subject to UV divergences, i.e., the integral in effect behaves as $\int d\varepsilon/\varepsilon$ leading to a logarithmic divergence due to the vacuum contribution. For a numerical solution this could be solved by a numerical cutoff acting as an effective regularization. To ensure the soundness of the numerical scheme, however, we must analyze this issue in more detail. From Eq. (11) we immediately obtain

$$\frac{\partial^2 \tilde{\chi}_3}{\partial t^2} + 4\varepsilon^2 \tilde{\chi}_3 = -\frac{4\varepsilon_\perp E}{\varepsilon} + 2E\tilde{\chi}_2. \quad (13)$$

For a modest plasma density, with a plasma frequency well below the pair-creation resonance (i.e., $\partial_t \ll 2\varepsilon$), the left-hand-side operator of Eq. (13) can be inverted to all orders in an expansion in the small operator $(1/\varepsilon)\partial_t$. Formally solving Eq. (13) for $\tilde{\chi}_3$ we get

$$\tilde{\chi}_3 = -D^{-1}\left(\frac{4\varepsilon_\perp E}{\varepsilon} - 2E\tilde{\chi}_2\right), \quad (14)$$

where the inverse operator is

$$D^{-1} = \left[1 - \frac{1}{4\varepsilon^2}\frac{\partial^2}{\partial t^2} + \left(\frac{1}{4\varepsilon^2}\frac{\partial^2}{\partial t^2}\right)^2 + \cdots\right]\frac{1}{4\varepsilon^2}. \quad (15)$$

Keeping only terms up to $\partial^2/\partial t^2$, we use Eqs. (14) and (15) in Eq. (11) to get an equation for the phase space current $\tilde{\chi}_1$,

which reads

$$\frac{\partial \tilde{\chi}_1}{\partial t} = 2\frac{\varepsilon_\perp^2}{\varepsilon^2}\frac{\partial^2}{\partial t^2}\left(\frac{E}{4\varepsilon^3}\right) + 4\varepsilon_\perp\left[\left(1 - \frac{1}{4\varepsilon^2}\frac{\partial^2}{\partial t^2}\right)\frac{E\chi_2}{4\varepsilon^2}\right]. \quad (16)$$

Finally, combining Eq. (16) with the time derivative of Ampère's law (12), we obtain

$$\frac{\partial^2 E}{\partial t^2}\left(\frac{1}{\eta_B} + 2\int \frac{\varepsilon_\perp^2}{\varepsilon^5}d^3 p\right)$$

$$= -\int 2\frac{\varepsilon_\perp^2}{\varepsilon^2}\left[2\frac{\partial E}{\partial t}\frac{\partial}{\partial t}\left(\frac{1}{\varepsilon^3}\right) + E\frac{\partial^2}{\partial t^2}\left(\frac{1}{\varepsilon^3}\right)\right]d^3 p - \frac{\partial j_p}{\partial t}, \quad (17)$$

where we have renamed $\eta = \eta_B$ to highlight that this corresponds to the bare value of the coefficient, obtained by using the bare value of the charge e_B, and noting that $\eta_B \propto e_B^2$. Here we have introduced the plasma current

$$j_p = \int 4\varepsilon_\perp\left[\left(1 - \frac{1}{4\varepsilon^2}\frac{\partial^2}{\partial t^2}\right)\frac{E\tilde{\chi}_2}{4\varepsilon^2}\right]d^3 p, \quad (18)$$

which is the part of the current that is proportional to the mass density. Recall that $\tilde{\chi}_2$ is defined as the deviation from the vacuum state, and thus new particles that are created will also contribute to the plasma current. However, our main concern here is the vacuum contribution of the left-hand side of Eq. (17), containing the the integral $2\int(\varepsilon_\perp^2/\varepsilon^5)d^3 p$ which has a logarithmic divergence. As deduced in Refs. [21,34], by introducing a regularization (i.e., a cutoff Λ_C in momentum space) and replacing the bare value of the electron charge e_B with the physically measurable one, e_R, according to

$$e_R^2 = \frac{e_B^2}{1 + \frac{e_B^2}{24\pi^2}\ln\left(\frac{\Lambda_C}{m}\right)} \quad (19)$$

Ampère's law gets its standard form. Since $\eta_B \propto e_B^2$, this corresponds to

$$\frac{1}{\eta_B} + 2\int^{\Lambda_C}\frac{\varepsilon_\perp^2}{\varepsilon^5}d^3 p = \frac{1}{\eta_B} + \frac{\ln \Lambda_C}{6} \to \frac{1}{\eta_R}. \quad (20)$$

The remaining part of the vacuum current, written on the right-hand side of Eq. (17), is nonzero but finite, due to the temporal variations of $\varepsilon(t) = m\{1 + p_\perp^2 + [q - A(t)]^2\}^{1/2}$. Moreover, as $\eta_R = \alpha/\pi \ll 1$, and the dynamics evolve on a timescale much slower than the Compton scale (i.e., $\partial/\partial t \ll 1$) the relative importance of the nonvanishing vacuum contribution, known as vacuum polarization, is small.

From a theoretical point of view, when the back-reaction in Ampère's law is included, it is important to confirm that the UV divergences can be handled by a renormalization. However, for our case to be studied, typically with a numerical cutoff of the order $\Lambda_C \sim 70$, and with $\eta = \alpha/2\pi^2$, the slow logarithmic divergence term gives a finite contribution that in practice is very small, of the order 0.002 of the plasma current or smaller. Accordingly, for the parameters used here, the difference between the bare charge and the measurable one is negligible. It should be stressed, though, that this conclusion is largely dependent on technical details. For a much larger numerical cutoff, or for an enhanced value of the fine-structure constant (as is sometimes used to speed up

numerical schemes; see, e.g., Ref. [21]), it could very well be necessary to use the renormalized expression. The above calculation shows that it is straightforward to do so also when applying the DHW formalism. However, due to the smallness of this correction for the parameters of our case, we have not done this in the numerical calculations that follow.

IV. NUMERICAL RESULTS

A. Preliminaries

Equations (11) and (12) are solved numerically using a phase corrected staggered leapfrog method [41]. While this is straightforward in principle, the full problem with three independent variables $\chi = \chi(q, p_\perp, t)$ is still numerically demanding when run on a standard workstation. One reason is the strongly relativistic motion (gamma factors sometimes exceeding 50) requiring a high value of the momentum cutoff q_c in q space of the order of $q_c \sim 100$. Typical parameters of the simulations are a time step of the order of $\Delta t \sim 0.001$, parallel momentum step $\Delta q \sim 0.01$, and perpendicular momentum step $\Delta p_\perp \sim 0.1$. In spite of the rather good resolution in parallel momentum, the q dependence of the produced data tends to look noisy. This is due to the Zitterbewegung effect, which produces increasingly short scales. Nevertheless, the dynamics of the larger scales are not sensitive to the small scale details, i.e., changing Δq does not affect the results presented in this paper.

That the numerical scheme produce sound results is confirmed by studying the energy conservation law. An energy conservation law of the system (11) and (12) can be written in the form

$$\frac{d}{dt}\left\{\frac{E^2}{2} + \eta \int [\tilde{\chi}_2 + (q - A)\tilde{\chi}_1]\,d^2p\right\} = 0. \quad (21)$$

Due to the back-reaction in Ampère's law, containing both the conduction current and polarization current [19,21], the energy density of the electric field is diminished at the same rate as the kinetic energy of the initial plasma and of the produced pairs grow. For the numerical resolutions used in the runs presented below, the total energy of the system is conserved within a relative error typically less than 10^{-4}. Note that the total energy includes also the growing rest mass energy due to particle creation.

As initial conditions in the runs we let $E(t = 0) = E_0$ and $A(t = 0) = 0$. Moreover, the normalized background variables for $t = 0$ are taken as

$$\tilde{\chi}_1 = \frac{2qf(q, p_\perp)}{(1 + q^2 + p_\perp^2)^{1/2}},$$

$$\tilde{\chi}_2 = \frac{2f(q, p_\perp)\varepsilon_\perp}{(1 + q^2 + p_\perp^2)^{1/2}}. \quad (22)$$

Here $f(q, p_\perp)$ is a Fermi-Dirac distribution,

$$f(q, p_\perp) = \frac{1}{1 + \exp[(\varepsilon - \mu)/T]}, \quad (23)$$

where μ is the chemical potential and T is the temperature (we normalize both μ and T with the electron mass). For $\mu \gg T$, the chemical potential fulfills $\mu \approx E_F$, where E_F is the Fermi energy, in which case the distribution will be
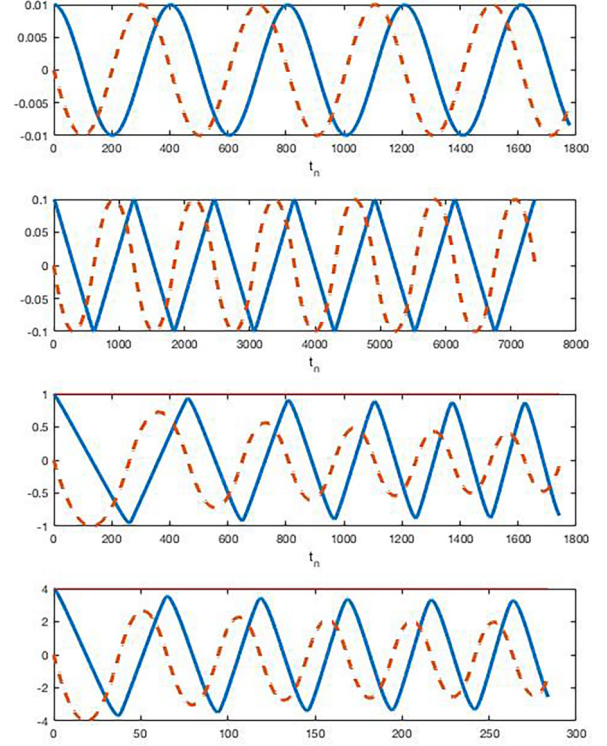

FIG. 1. The normalized vector potential A_N, the dashed lines, and electric field E, the solid lines, vs the normalized time $t_n = \omega_c t$ for four different values of initial E field $E = (0.01, 0.1, 1, 4)$.

degenerate (i.e., we will have $f \approx 1$, i.e., all electron states filled, for energies smaller than the Fermi energy, and $f \approx 0$ otherwise). Naturally, nondegenerate initial distributions are still possible when using Eq. (23), by letting $\mu < T$. Also, by picking a large but negative chemical potential, we get a Maxwell-Boltzmann type of distribution.

B. Plasma oscillation dynamics

In Fig. 1 the electric field and vector potential are plotted for different values of E_0, μ, and T. To be able to show the evolution of A in the same plot as E, we have normalized the vector potential once more, displaying $A_N = E(t = 0)A(t)/A_{\text{peak}}$, where A_{peak} is the peak absolute value of $A(t)$. Even in the upper panel, with a comparatively modest field strength, $E(t = 0) = 0.01E_{cr}$, $\mu = 1$ and $T = 0.1$, we have nonlinear relativistic motion with $A_{\text{peak}} = 1.85$ (essentially once the motion becomes relativistic, A_{peak} corresponds to the peak gamma factor during an oscillation cycle, averaged over all particles). In spite of the relativistic motion, the deviation from linear behavior is not clearly visible in the temporal field profile, although a careful analysis would show a harmonic content in the spectrum. However, changing the initial electric field to $E(t = 0) = 0.1E_{cr}$ (still with $\mu = 1$ and $T = 0.1$), the moderately relativistic motion turns into strongly relativistic oscillations (with $A_{\text{peak}} = 15.9$. The oscillation is still perfectly periodic, as seen in the second panel of Fig. 1, but now there is a clear sawtooth profile of the electric field. This effect comes from the strong relativistic motion, where the gamma factors are much larger than unity for most of the oscillation,

except at the turning points. As a result, for most of the oscillations, all particles move close to the speed of light, giving a current that is more of less constant until it changes direction. Given this, the sawtooth profile of the electric field is a direct consequence of Ampère's law. Moreover, due to the strong relativistic motion, the effective (nonlinear) plasma frequency is much lower, due to the high gamma factors giving the electrons a large effective mass.

However, the results in the two upper panels do not deviate much from a computation based on the relativistic Vlasov equation (in the standard classical version of plasma physics; see, e.g., Ref. [40] for a comparison of quantum and classical versions of the Vlasov equation). To see quantum relativistic physics, we need to approach the Schwinger critical field, i.e., let $E(t = 0) \sim 1$. In the third panel, we have used $E(t = 0) = 1$, $\mu = 1.5$, and $T = 0.2$. Here we still see a sawtooth profile for the electric field as expected, since $A_{\text{peak}} = 67.2$. However, we now also have pronounced decrease of the vector potential for each oscillation. While the electric field also decreases, we note that A decreases more rapidly than E. With $E = -\partial A / \partial t$ the more rapid decrease of A is consistent with an increase in the plasma frequency. While the energy loss of the electric field due to pair production is clearly seen, the increase in plasma frequency (due to the increased number density) is even more pronounced. The latter effect is seen both in the relation between E and A, and by observing the gradual change in time period between successive peaks.

Finally, in the fourth panel, by picking $E(t = 0) = 4$, $\mu = 4$ and $T = 0.2$, corresponding to $A_{\text{peak}} = 39.7$ we have displayed the dynamics of the plasma oscillation in a regime well beyond the Schwinger critical field. The curve might look surprisingly similar to the third panel with $E(1 = 0) = 1$, with the same type of energy loss and decrease in frequency. However, from the temporal scale we see that here the oscillation frequency is much higher, due to the higher value of the electron number density. Hence the energy loss due to pair production is indeed more rapid with a higher initial electric field, as expected.

That the energy loss and frequency increase is the result of electron-positron pair production can be confirmed by investigating the evolution of the total particle (electron and positron) number density n. In terms of the normalized χ variables, n can be expressed as [35]

$$n = \frac{1}{(2\pi)^3} \int \frac{1}{\varepsilon} [\varepsilon_\perp \tilde{\chi}_2 + (q - A)\tilde{\chi}_1] d^2 p. \qquad (24)$$

Plotting the quantity $n(t)/n(t = 0)$ in Fig. 2, for the same initial data used in the four panels of Fig. 1, we see that there is as a gradual increase of particles in panels 3 and 4, consistent with the energy loss and increase of plasma frequency seen in the corresponding panels of Fig. 1.

At the same time, it is also of some interest to note the fast but small-scale oscillations of n seen in panels 1 and 2. At the peak of the number density in the oscillation cycle, the particle data is noisy, due to Zitterbewegung creating small scales in momentum space. The increase in particle density, however, is reversible, and thus there is no long-term gradual particle increase. Thus, in what follows, when we speak of pair production, we will be referring to the accumulative process seen
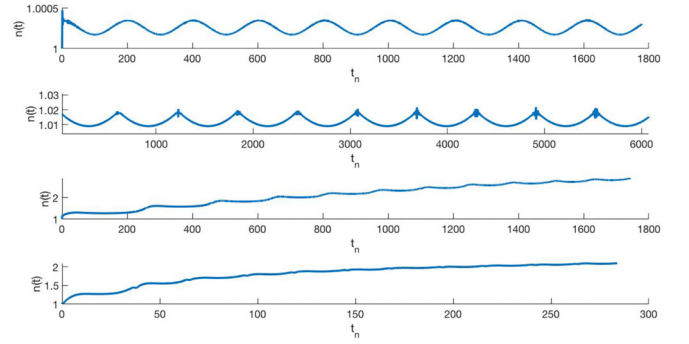

FIG. 2. The total particle number density $n(t)$ over time for four different initial values of the electric field $E(t = 0) = (0.01, 0.1, 1, 4)$.

in panels 3 and 4, rather than the reversible small-amplitude oscillations seen in panels 1 and 2.

Interestingly, the damping of the electric field is relatively modest even when the pair creation is rather high, as seen when comparing the third and fourth panels of Figs. 1 and 2. The reason is that the energy loss by creating low-energy pairs is of the order of two rest mass energies, whereas the characteristic energy of the plasma particles is much higher, larger by a factor γ_{char}. Here the characteristic value of the γ factor typically is ~ 35 (with the corresponding peak value $\gamma_{\text{peak}} \sim 70$). As a result significant creation of low-energy pairs can take place without heavy damping.

Furthermore, in regard to Fig. 2, while the relative increase in number density is somewhat higher in panel 3 as compared to panel 4, the pair production is considerably more rapid for the higher field, as can be seen when comparing the temporal scales. Finally, we note that there is a saturation of the number density in panels 3 and 4. For a lower field intensity, the decreasing field strength is a partial explanation, but for a higher field strength, the saturation of the damping is mostly due to the created pairs filling the available low-energy states (Pauli blocking). In this context, see, e.g., Refs. [21,31], where the difference between scalar and spinor QED is studied, starting from vacuum. We will come back to the issue of the energy spectrum of the created pairs; see Figs. 3 and 7.

For the case of a plasma initially present, there is no need to have the initial energy stored in the electric field. Starting instead with a sufficiently strong plasma current, that is with a kinetic energy density of the order $\sim \varepsilon_0 E_{\text{cr}}^2 / 2$, the kinetic energy will be converted into an electric field, and the pair production will set in. In Fig. 4 the evolution of the electric field and the vector potential is plotted for the initial conditions of $p_d = 70$, $E = 0$, $\mu = 3$, and $T = 0.2$. Here p_d is the kinetic drift momentum of the electrons relative to the stationary ions; i.e., in Eq. (23), we have replaced $\varepsilon \to \sqrt{1 + p_\perp^2 + (p_z - p_d)^2}$. For comparison, the results are compared with similar oscillations starting from no initial drift but with $E = 1$, $\mu = 1.5$, and $T = 0.2$. Once the kinetic energy has been converted into an electric field of the order of the Schwinger critical field, the pair creation dynamics shows a similar type of damping and frequency up-shift as seen in the plots starting from an electric field and a zero current. A few differences between the two sets of curves, although relatively
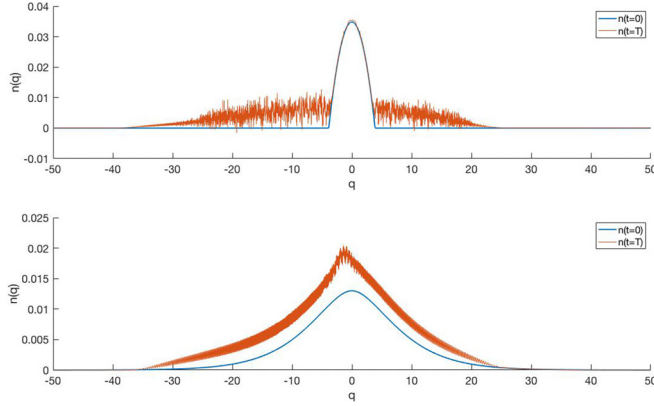
FIG. 3. The number density $n(q) = \int dp_\perp p_\perp / \varepsilon [\varepsilon_\perp \chi_2 + (q - A)\chi_1]$ as a function of the canonical momentum q is plotted for $E = 4$ for two cases: $\mu = 4$ and $T = 0.02$ (top panel) and $\mu = -10$ and $T = 5$ (bottom panel).

minor ones, can be noted. The most obvious is that the number of pairs created is a bit larger in the case with no initial drift (lower panel). As a result, the damping of the plasma oscillation is somewhat less pronounced (upper and middle panel). This is not a result of much physical significance, though, as the exact details of the evolution depend on the combination of all initial parameters. It was necessary to pick a higher value of μ and hence a higher plasma density, for the case of a drifting plasma, in order to get peak electric field of the same order. Nevertheless, the overall conclusion is that the qualitative dynamics is independent of the initial phase chosen for the plasma oscillation.
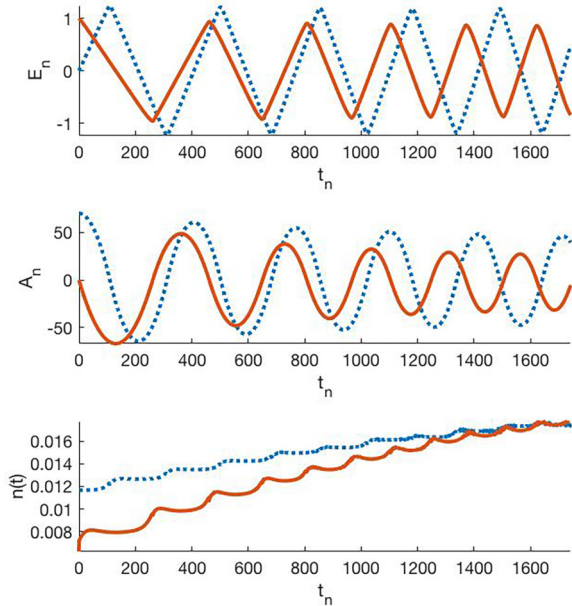

FIG. 4. The electric field (upper panel), vector potential (middle panel), and number density (lower panel) for a plasma with an initial current. The dotted line (blue) corresponds to the initial parameters $E = 0$, $\mu = 3$, $T = 0.2$, and $p_d = 70$. The solid line (brown) corresponds to initial values $E = 1$, $\mu = 1.5$, $T = 0.2$, and $p_d = 0$.

C. Analytical estimates

In order to gain some qualitative understanding, let us make certain analytical estimates of the pair-creation process. While we are interested in the dynamics with an initial plasma present, let us first consider the pair-creation rate starting from vacuum. As long as the available particle states are free to be filled, the pair-creation rate dn/dt, is given by (see Refs. [5,6])

$$\frac{dn}{dt} = \frac{1}{4\pi^3 c} \left(\frac{eE}{\hbar}\right)^2 \exp\left(-\frac{\pi E_{cr}}{E}\right). \tag{25}$$

For electrical fields well above the critical field, in normalized units, we thus have

$$\frac{dn}{dt} \sim \frac{E^2}{4\pi^3}, \tag{26}$$

which should be applicable as an order of magnitude estimate also for $E \gtrsim E_{cr}$. Since the created particles will move close to the speed of light soon after creation, the current generated from the pairs can be written as $j \sim \int_0^t (dn/dt')dt'$, such that

$$\frac{dE}{dt} \sim -\frac{\alpha}{\pi^2} \int_0^t E^2 \, dt'. \tag{27}$$

Taking the time derivative of Eq. (27), replacing the estimate with an equality, using dE/dt as an integrating factor, the resulting equation turns out to be separable and can therefore be solved exactly by elementary means. If we ignore the uncertainty implied in Eq. (27), the time T_p to completely convert the electric field energy to particle energy is given by $T_p = \sqrt{(3/2)} I\pi / (\alpha E_0)^{1/2}$, where the integral I is given by $I = \int_0^1 (1 - x^3)^{-1/2} \, dx \approx 1.4$. This estimate for the conversion time is consistent with the results presented in Refs [31,42,43]. Noting that T_p constitutes a quarter of an oscillation cycle, the implied oscillation frequency is of the order

$$\omega = \frac{1}{\sqrt{6}I} (\alpha E_0)^{1/2} \sim 0.3 (\alpha E_0)^{1/2}, \tag{28}$$

where E_0 is the initial electric field. It can be noted that the above estimate is in very good agreement with Fig. 10 below, which is a obtained from a numerical computation starting from vacuum (the period time for $E_0 = 100$ is around $T_P \approx 18$, which is within 10% accuracy of the given estimate; see Sec. IV E for details) Naturally, the oscillation frequency with a plasma present can be substantially higher (if we have sufficient number of particles initially present) than the "initial vacuum frequency" given here. However, in the case the oscillation frequency due to the initial plasma is much higher than Eq. (28), the particles created during an oscillation cycle will be close to negligible compared to those present initially.

Moreover, given the frequency scale, we can estimate the peak γ factors during an oscillation. We denote the peak value with γ_p and note that typically $\gamma \sim p_z$. Naturally, this estimate is particularly accurate for the peak value γ_p during an oscillation cycle, but it should be noted that $p_z \gg 1$ and $p_z \gg p_\perp$ holds for the majority of the particles and for the majority of an oscillation cycle. As a result, we can estimate $\gamma_p \sim \int_0^T E(t) \, dt \sim E_0/\omega$. Thus it follows that the average γ

factor during a cycle $\langle\gamma\rangle$ will roughly be

$$\langle\gamma\rangle \sim \frac{\gamma_p}{2} \sim \frac{E_0}{2\omega} \sim \frac{3}{2}\left(\frac{E_0}{\alpha}\right)^{1/2}. \tag{29}$$

Moreover, the number density n_0 that have been created imply a plasma frequency ω_p^2 (with $\omega_p^2 \equiv 4\pi\alpha n/m$, not accounting for the relativistic frequency lowering of the frequency. As is well known, the oscillation frequency will differ from the plasma frequency due to relativistic effects, which is captured by replacing the mass with the effective mass, i.e., by making a substitution $m \to m\langle\gamma\rangle$. Thus, using the above estimates we obtain

$$\omega_p^2 \sim \omega^2\langle\gamma\rangle \sim \tfrac{1}{6}\alpha^{1/2}E_0^{3/2}. \tag{30}$$

With a plasma initially present, if the value of ω_p^2 at $t = 0$ is much larger than $\sim\alpha^{1/2}E_0^{3/2}/6$, naturally the influence on the plasma dynamics due to the Schwinger mechanism will be comparatively modest. Nevertheless, the accumulated effect during a large number of periods may still be noticeable.

Next we assume, for the sake of the argument, that the initial plasma number density $n_0 = n(t = 0)$ is of the same order as the Schwinger induced contribution after an oscillation period. This case is considered in the two lower panels of Figs. 1 and 2, and as a consequence we see that the plasma density roughly increases by a factor 2 during the first oscillation period. While this implies a substantial increase in both the plasma density and the oscillation frequency, interestingly we see that the damping of the plasma oscillation still is relatively modest, as shown by the electric field evolution. To understand this, for simplicity we concentrate on the specific case with $E(t = 0) \sim 1$, in which case the pairs will be generated with initial energies $\simeq 2m$. Thus for each created pair, the plasma oscillation energy will decrease by an amount of the order $\sim 2m$. However, subsequent acceleration of the pairs just converts the electrostatic plasma oscillation energy into kinetic plasma oscillation energy. As a result, no further damping occurs due to acceleration of the created pairs. Thus we can estimate the relative drop in plasma oscillation energy during a period as

$$\frac{\delta W}{W} \sim \frac{\delta n_0}{\langle\gamma\rangle(n_0 + \delta n_0)} \sim \frac{\delta n_0}{(n_0 + \delta n_0)}\frac{2\alpha^{1/2}}{3E^{1/2}}, \tag{31}$$

where δn_0 is the change in number density after an oscillation cycle. This shows that even with a substantial increase in particle number density and wave energy, i.e., with $\delta n_0 \sim n_0$, the decrease in wave energy during an oscillation is only a few percent for E of the order unity. Moreover, for $E > 1$, the damping of the plasma oscillation amplitude will not increase with the initial electric field, but rather the opposite. Naturally, for $E < 1$, the exponential dependence included in Eq. (25) will suppress the influence of the Schwinger mechanism.

As seen in Figs. 1 and 2, and confirmed by the present analysis, the change in oscillation frequency is a much more pronounced effect than the plasma oscillation damping (i.e., the energy loss as captured by the decreasing peak electric field), which explains why the vector potential A falls off more rapidly than the electric field. As an order of magnitude estimate, the relative increase in frequency during an oscillation
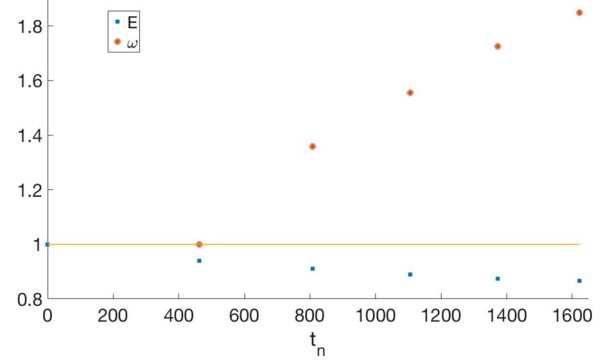

FIG. 5. The electric field damping (squares) and frequency increase (dots) for $E(t = 0) = 1$, $\mu = 1.5$ and $T = 0.2$, where a line equal to unity is drawn for comparison. The electric field dots are evaluated at successive peaks, and the frequencies are computed as $\omega = 2\pi/T_p$, with the time period T_p computed for successive peak values of the electric field. The frequencies are normalized against the frequency for the first oscillation period (with $T_p = 462$).

period is

$$\frac{\delta\omega}{\omega} \sim \frac{\delta n_0}{(n_0 + \delta n_0)} \sim \frac{E^{1/2}}{\alpha^{1/2}}\frac{\delta W}{W}. \tag{32}$$

The above scaling can be deduced using $\omega^2 \sim \omega_p^2/\langle\gamma\rangle$ together with $\delta\omega/\omega \sim -\delta\langle\gamma\rangle/\langle\gamma\rangle$, as follows from Eq. (29), given that changes of the electric field amplitude is proportional to $\alpha^{1/2}$ from Eq. (31).

In order to illustrate the validity of the estimates provided here, next we compare the magnitude of the frequency increase with the magnitude of the damping rate. That the frequency upshift is indeed a more pronounced effect than the damping [larger by a factor $E^{1/2}\alpha^{-1/2}$, as described by Eq. (32)] is illustrated in Fig. 5, where the pair-creation damping and frequency up-shift have been evaluated for the same parameters as in panel 3 of Fig. 1. We note that the electric field is reduced by roughly 10% after five oscillation periods, whereas the frequency has been nearly doubled during the same time. Although in the next subsection we will study wave damping in more detail, we note that the scaling relation (32) can be used to provide a rough estimate for the corresponding frequency upshift.

D. Plasma oscillation damping

The damping of plasma oscillations and the increase in plasma frequency, due to electron-positron pair-production, is the main focus of our work. While the estimates provided in the previous subsection will give a rough idea of the scaling, important effects such as Pauli blocking preventing pairs from being created is not accounted for.

First of all, we would like illustrate the mechanism of Pauli blocking. This mechanism is always present in the DHW formalism. However, whether or not it is an important feature dynamically, depends on the number of free states where pairs can be created. In particular, a degenerate initial distribution will block the low-energy states in momentum space, which is the region where particles are most easily created. This feature is on display in Fig. 3. In the upper panel we have considered
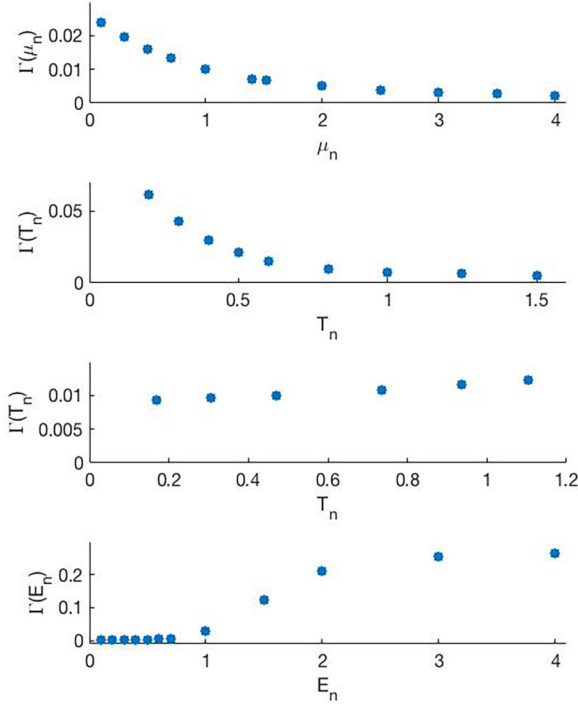
FIG. 6. The damping of the electric field Γ as a function of three different parameters. In the top panel we plot Γ vs μ for $E = 1$ and $T = 1$. For the second panel, we plot Γ vs the temperature T for $E = 1$ and $\mu = 1.5$. For the third panel, we vary T but compensate with varying μ to keep the number density fixed. Finally, in the bottom panel, we plot Γ vs initial electric field for $T = 0.4$ and $\mu = 1.5$.

a degenerate distribution with $\mu = 4$ and $T = 0.02$, where all the low-energy electron states are filled, preventing further pair creation in the filled region. As shown, due to a strong initial field $E_0 = 4$, pairs are still created at a high rate, but the low-energy region is perfectly blocked, as seen by comparing the momentum distribution $n(q)$ after an oscillation period with the the initial momentum distribution. Specifically, it should be noted that the two curves coincide (no further pair-creation) for a low or modest parallel momentum. By contrast, for an initial distribution far from degeneracy, $\mu = -10$ and $T = 5$, the corresponding comparison (lower panel of Fig. 3) shows that the blocking is not a feature, i.e., new pairs are created everywhere in momentum space.

With the basic mechanism of Pauli blocking established, we will next study how the pace of the damping scales with the plasma parameters (the temperature and the chemical potential) as well as the initial electric field strength. We define the relative one-period electric field damping Γ as

$$\Gamma = \frac{|E(T_p) - E(t = 0)|}{E(t = 0)}, \tag{33}$$

where T_p is the period time of the first oscillation. In Fig. 6 the damping Γ is plotted for different values of E, μ, and T. In the upper panel of Fig. 6, we use the initial electric field $E(t = 0) = 1$, a temperature $T = 1$, and a varying μ. We see that there is a clear decay in the damping rate with increasing chemical potential. The main reason for the decay in damping with μ is due to the increase in plasma frequency, since the level of damping is computed after a plasma pe-

riod, but the energy loss rate is only weakly dependent of the plasma frequency. In the second panel, where μ is fixed but the temperature is varied, there is a similar effect, as the particle density grows with T for a fixed μ. In principle, we could expect a reversal of this mechanism for low temperature, as there would be no free low-energy states to create pairs for a fully degenerate system. While this mechanism certainly is present in principle, we cannot see the effect for this value of μ, as the particle density is too low to block a sufficient volume in momentum space.

In order to investigate the effect of blocked low-energy states on the damping rate, in the third panel we vary the temperature. However, varying the temperature while keeping μ fixed leads to an increased plasma frequency. Thus, in order to focus only on the shape of the electron distribution, we instead keep the number density fixed, which requires us to lower the chemical potential μ when increasing T. Contrary to the second panel in Fig. 6, we now see an increase in Γ with temperature. In agreement with the results shown in Fig. 3, this can be explained as a partial pair-production blocking for the colder system, with fewer empty low-energy states available where pairs can be produced.

Finally, in the fourth panel of Fig. 6, for $\mu = 1.5$ and $T = 0.4$, we see a rapid increase in Γ as the initial electric field approaches and pass the critical field. At first one may be a bit surprised to see the saturation in damping occurring for $E(t = 0) \sim 3$–4. However, it should be noted that the energy loss rate after a cycle is $\propto E^2 \Gamma$, such that even if Γ is more or less saturated, the pair-production rate continue to increase with the field $\propto E^2$.

Next, there is a question where in the momentum space the new pairs are produced. In Fig. 7 contour curves over the integrand in Eq. (24) is shown, $n(p_\perp, p_z)$, where we have switched back to kinetic momentum p_z rather than canonical momentum q. The upper panel shows the contour curves for the initial Fermi-Dirac distribution. A quarter of a plasma period later, we can clearly distinguish the initial particle distribution. As can be seen, the initial particles has been shifted a distance $\approx A(t)$ in the p_z direction, but with a more or less conserved shape. However, in addition to the original particles, a contribution from electron-positron pairs have been added, accelerated by the fields to have a much larger parallel momentum than perpendicular momentum. For a more detailed discussion about the parallel and perpendicular momentum distribution of the produced pairs see Ref. [44]. Note that after a quarter period, the produced pairs have larger negative p_z momentum than the original particles. In the lower panel, after a half cycle, the symmetry has been restored, as the produced pairs are located on both sides (in parallel momentum space) of the original particles. As the pair-production process continues, eventually it will be difficult to separate the original particles from the newly produced ones, as the produced particles will outnumber the original ones.

Before we end the discussion of the pair-creation dynamics in the presence of plasma, let us point out that there are interesting papers of relevance in this context by Refs. [45,48]. First, in Ref. [45], the authors consider an initial plasma in the context of Schwinger pair-production. However, rather than studying an electrostatic field, they compute the damping of an electromagnetic wave due to the energy loss through
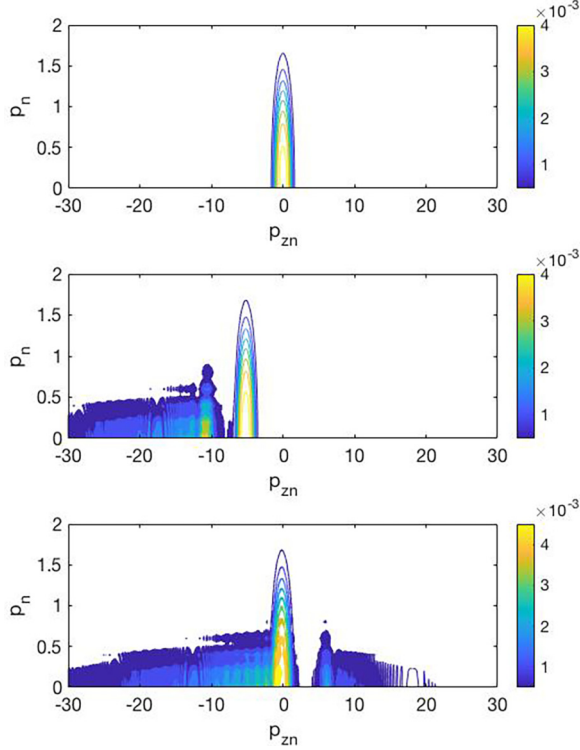
FIG. 7. Color mappings of the momentum distribution of the total particle density $n(p_z, p_\perp)$ at three different times $t = (0, T_p/4, T_p/2)$ for $E_0 = 1$, $\mu = 1.5$, and $T = 0.2$.

the Schwinger mechanism. However, in contrast to our study, that paper considered a cold plasma with a delta function for the initial momentum distribution, which limits the potential applicability to rather modest plasma densities (with a small Fermi momentum) and temperatures.

Finally, in Ref. [48], production of pairs by electrostatic waves in plasma was studied using a relativistic quantum fluid model assuming that the electric field varies slowly in comparison with the Compton frequency. While the overall pair production rate used in hydrodynamics based on the Schwinger theory (proportional to $\exp[-\pi E_{cr}/(E)]$) is consistent with the DHW formalism, the kinetic details (e.g., where in momentum space the pairs are created) are important for the plasma oscillation properties. More specifically, many features seen in our treatment such as Pauli blocking, cannot be covered in a hydrodynamic approach. Nevertheless, the more modest computational demands makes hydrodynamical studies a good complement to kinetic treatments, which is illustrated by the fact that the spatial influence also could be covered in Ref. [48].

E. The initial vacuum regime

Up to now we have considered pair-creation dynamics in the presence of a plasma. By contrast, previous works of a similar nature, e.g., Refs. [21,22,25–29,31], have been focusing on pair-creation dynamics when starting from a vacuum state. In this case, naturally one cannot begin by postulating a plasma oscillation with a fixed amplitude as initial condition, as there is no initial plasma. Instead one has to use an external

electric field starting up the process, either in the form of a time-dependent Sauter pulse [32] or by imposing a constant external field at $t = 0$. In spite of these differences, once the plasma is created, many of the features seen in the present paper when considering a plasma are the same as those seen in previous works starting from vacuum. In particular, the plasma oscillation amplitude tend to diminish gradually and the plasma oscillation frequency increases due to pairs being gradually created [18,19,21].

However, starting from vacuum is numerically more challenging than studying the physics of a high-density plasma, due to the very large parallel momenta induced by a field close to the Schwinger limit, unless the initial plasma density and thereby plasma frequency is high. As a result, most previous numerical works have simplified the numerical schemes in various ways. For example, some works (e.g., Refs. [19,22]) limited the treatment to include no perpendicular momentum dependence in the calculation. While several of the previous works (e.g., Ref. [21]) account also for the dependence on perpendicular momenta, importantly, most previous calculations starting from vacuum and including the back-reaction through Ampère's law have simplified the numerics by using a fine-structure constant that is much larger than the actual value. As it turns out, this choice limits the peak parallel momentum rather drastically. This is not entirely unproblematic when a complex dynamical situation is studied. While the basic physical mechanisms does not change when using a magnified α, the relative importance of the dynamical mechanisms will not stay the same.

In order to compare with previous works, particularly Ref. [21], we have started the dynamics with an external Sauter pulse [46] of the form

$$A_{ex}(t) = A_0 \left[1 + \tanh\left(\frac{t - t_0}{\tau}\right) \right], \quad (34)$$

$$E_{ex}(t) = -\frac{A_0}{\tau \cosh^2\left(\frac{t - t_0}{\tau}\right)} \quad (35)$$

and used the actual value of the fine-structure constant $\alpha = 0.007297$ with $\eta = \alpha/(2\pi)^2$. Starting the numerical computation at $t = 0$, we let $t_0 = -2$ in all our runs, to include a short build-up phase of the Sauter pulse. For the above case, the tendency is that almost all pair creation happens in the very first initial stage, much shorter than a plasma period, before any plasma oscillations can be seen.

This is illustrated in Fig. 8, where we consider a pulse with $A_0 = 10$ and $\tau = 0.5$. As can be seen in the upper panel, the self-consistent field is strong (peak electric field around $0.6E_{cr}$), but no visible pair creation is done by the self-consistent field that is responsible for the plasma oscillation. In particular, the peak electric field of the Sauter pulse is far from recovered, and the extra pair creation that takes place after the initial phase is more or less negligible, as seen from the constant number density in the lower panel.

As our next step, in order to illustrate the influence of a modified value of α on the dynamics, we consider an enhanced value of the fine-structure constant. For this purpose, we match the parameters of Ref. [21], also accounting for the charge renormalization (with a cutoff value $\Lambda_C = 25$), the
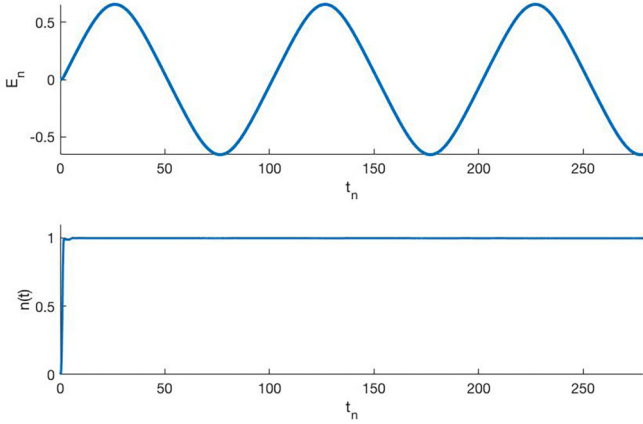
FIG. 8. The induced electric field (i.e., without including the external field of the initial Sauter pulse) (upper panel) and the induced number density (lower panel). The parameter values for the Sauter pulse are $A_0 = 10$ and $\tau = 0.5$

FIG. 10. The electric field profile starting from a an initial value $E(t = 0) = 100 E_{cr}$ using the actual value of α. The result is compared with the curve computed in Ref. [30], using the same parameters. The data from [30] have been extracted using the online tool WebPlotDigitizer [49].

magnified value of the coefficient in Ampère's law become $\eta = 0.26$ [as compared to $\eta = \alpha/(2\pi^2) \approx 0.3697 \times 10^{-3}$]. In Fig. 9 the electric field and pair density is shown for a Sauter pulse with initial parameters $A_0 = 10$ and $\tau = 0.5$. With a peak field of $E \sim 15$, and a similar oscillation frequency and decay in the upper panel as previously found by Ref. [21], there is close resemblance to results computed for a magnified value of α. In the lower panel of Fig. 9, we see the evolution of the number of pairs. While much of the particles are created by the initial Sauter pulse, there is subsequent significant pair creation due to the plasma field (generated by the back-reaction), accompanied by further damping of the electric field. However, as is apparent from a comparison with Fig. 8, the dynamics depend rather sensitively on the value of α.
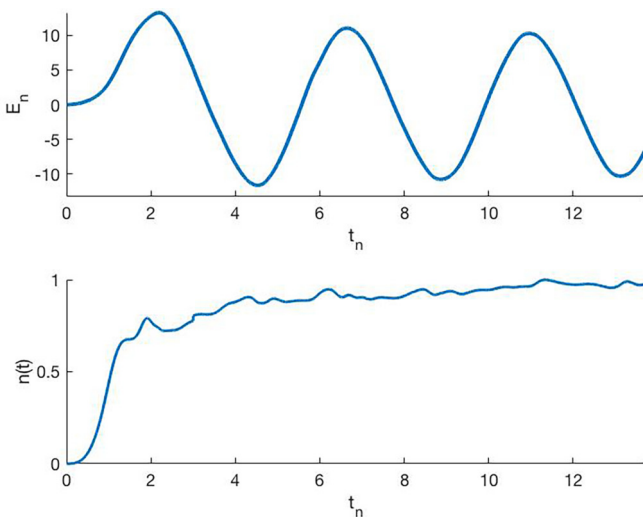

FIG. 9. The induced electric field (i.e., without including the external field of the initial Sauter pulse) (upper panel) and the induced number density (lower panel). The parameter values for the Sauter pulse are $A_0 = 10$ and $\tau = 0.5$ and the enhanced value $\alpha = 4$ for the fine-structure constant.
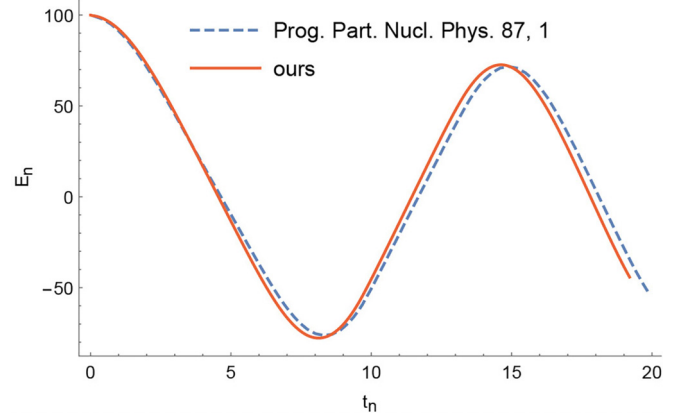
While the use of a magnified fine-structure constant has been rather common in the research literature when starting from vacuum, some works (e.g., Refs. [26,30]) have used the actual value. Specifically, we now compare our results with those of [30]. Here the authors started from a homogeneous electric field as initial condition (rather than a Sauter pulse). This is a numerically challenging problem, due to large relativistic factors (requiring a large volume in momentum space) combined with the distinct separation of timescales, with the Compton scale being much shorter than the plasma oscillation time scale. However, for very strong initial fields, the problem turns out to be less demanding computationally, as the separation in timescales is not equally pronounced. To confirm the agreement with previous works in this regime, we have used a very strong initial field $E(t = 0) = 100 E_{cr}$, together with the actual value of α, and compared the electric field profile with the curve shown in Ref. [30] using the same parameters; see Fig. 10. While there is a small but visible difference between the two curves, the deviation is not larger than should be expected with regard to the numerical precision.

As the dynamics when the back-reaction is prominent (for a discussion of when back-reaction can be neglected; see, e.g., Refs. [42,43]) tend to depend on the actual value of the fine-structure constant, it would be of interest to systematically reconsider many of the studies made using a magnified value of α. Since this tends to be computationally demanding, and our main focus has been on the regime with an initial plasma, a more complete study of the initial vacuum regime is outside the scope of the present paper.

V. RADIATION REACTION

In this section we will consider potential mechanisms that have been omitted, but may compete with the processes considered up to now. In the overall dynamics, the main effects of pair production is a frequency increase of the plasma oscillations, together with damping. The present DHW model is an accurate description of the mean-field physics, but processes

converting energy from coherent degrees of freedom to non-coherent degrees of freedom is not covered. For high plasma densities, we note that in principle it is possible that certain incoherent processes outside the mean-field description can be suppressed due to many-particle effects. For a concrete example illustrating the interplay between long-scale collective phenomena and short-scale incoherent processes; see, e.g., Fig. 1 in Ref. [47].

Specifically, single-particle radiation emitted by accelerated particles can be suppressed when the generated frequencies ω_e fulfill $N \equiv nc^3/\omega_e^3 \gg 1$, indicating that a large number of electrons N simultaneously interact with the same photon quanta. A precise estimate of the characteristic frequency ω_e would require substantial research, considering that the emission depend on the details of the particle distribution and may vary significantly during the oscillation period. Here we just note that soft emission (with $\omega_e \ll \omega_c$) generally will have $N \gg 1$, in which case collective interaction captured in the mean-field description will suppress single-particle effects. However, due to field strengths of the order the critical field, and a spread in perpendicular momentum not much smaller than m, a significant part of the emitted spectrum is likely to have frequencies ω_e of the order ω_c or possibly higher, implying $N < 1$, in which case single-particle emission gives an extra energy loss mechanism for the plasma oscillations not captured by the DHW model. Accordingly, in what follows, we will assume that single-particle emission is present and estimate the energy loss of the plasma oscillations based on this.

Next we note that the single-particle photon emission implies an effective friction-like force, where the standard expression is referred to as the Landau-Lifshitz force [50]. Here we limit the discussion to classical radiation reaction. Although the regime of study is well outside the classical limit of validity, this would suffice to produce an order of magnitude estimate. Moreover, it should be noted that more general QED calculations [51,52] involve large perpendicular momentum and electromagnetic fields, i.e., those calculations are not applicable to the electrostatic geometry with predominately large parallel momentum. This force scales as γ^2 and tend to be important when the field is strong enough to induce large particle energies. However, to a large degree, this effect is suppressed in a 1D electrostatic geometry, when the large gamma factor only comes from the motion parallel to the field. However, also in this case there is a finite contribution that survives, due to the particle spread in momentum. Using the classical Landau-Lifshitz expression [50] for the radiation reaction force $\mathbf{F}_{\rm rad}$, with the present normalizations and the given field geometry, the expression reduces to

$$\mathbf{F}_{\rm rad} = \frac{2\varepsilon}{3}\alpha\left[\left(\frac{\partial E}{\partial t} + \frac{E^2 p_z}{\varepsilon^2}\right)\hat{\mathbf{z}} - \frac{E^2 \varepsilon_\perp^2}{\varepsilon^2}\mathbf{p}\right]. \quad (36)$$

Next, we estimate the energy density loss due to the particle self-interaction during a plasma period. Dropping the term proportional to the time derivative of the electric field in Eq. (36) (as this contribution is considerably smaller in the strong field regime of interest here), the energy loss rate

$d\Delta W/dt$ of the plasma oscillation energy is given by [53]

$$\frac{d}{dt}\Delta W = \langle \mathbf{F}_{\rm rad} \cdot \mathbf{v}\rangle \approx \frac{2}{3}4\pi\alpha^2 n_0 E^2\langle p_\perp^2\rangle. \quad (37)$$

Here $\langle...\rangle$ denotes averaging over the particle distribution. It can be noted that the number density n_0 is related to the oscillation frequency (as seen, e.g., in Fig. 1), according to $4\pi\alpha n_0 = \omega_p^2 \sim \omega^2\gamma$, where n_0 is the number density in the laboratory frame, and γ is the characteristic relativistic factor of the particles averaged over a wave period. Using Eq. (37), the relative energy loss $\Delta W_P/W$ during an oscillation period can be estimated as

$$\frac{\Delta W_P}{W} \sim \frac{4\pi\alpha^2 n_0}{\omega} \sim \alpha\frac{\omega_p^2}{\omega}. \quad (38)$$

Here we have used $\int(E^2(t)dt/E^2(t=0)) \sim 3/\omega$ (a sinusoidal field profile averaged over a cycle gives a numerical factor π/ω, whereas an ideal sawtooth profile gives $2\pi/3$). Moreover, we have estimated $\langle p_\perp^2/m^2\rangle \sim 1/2$ for the plasma parameters typically used. Using $\omega_p^2/\omega \sim \omega\gamma$, and the Lorentz-force equation $dp_z/dt = E$, we can estimate $\gamma \sim p_z \sim E/\omega$ and hence

$$\frac{\Delta W_P}{W} \sim \alpha E. \quad (39)$$

Thus for E of the order of the critical field, the energy loss per oscillation period scales as α rather than $\sqrt{\alpha}$ as for the Schwinger mechanism. While this suggests that radiation reaction gives a smaller effect, comparing with Fig. 6 we see that for the actual value of α, we cannot be certain.

On the other hand, we note that an estimate based on the classical expression (36) tends to overestimate the loss rate as compared to a more accurate calculation based on QED; see e.g., [54]. This is captured in the so-called Gaunt factor G, which describes the quantum reduction in the energy loss rate. This is usually used in cases with large perpendicular momenta (for which a general field appears as a crossed field), while in our case we have large longitudinal momentum instead. Nevertheless, Fig. 14 of Ref. [54], where the standard $G(\chi_e)$ is plotted, suggests that the quantum corrected result significantly reduces the classical estimate for $\chi_e := \sqrt{-(F^{\mu\nu}p_\nu)^2}/(mE_{cr}) = Ep_\perp/mE_{cr} \sim 0.5$–1. Here $F^{\mu\nu}$ is the electromagnetic field tensor and p_ν is the 4-momentum.

Naturally, for electric field strengths well below the critical field, the exponential suppression of the pair-creation rate will make radiation losses dominant. For further results concerning field depletion due to radiation losses, see, e.g., Ref. [55].

To conclude, we expect that for fields of the order of the critical field, the inclusion of radiation reaction would not significantly modify the plasma oscillation dynamics, even though the damping due to pair creation is not necessarily stronger than that due to radiation losses (compare, e.g., Fig. 1). For the case when both mechanisms are small, however, to leading order the plasma oscillation energy loss can be computed perturbatively as the sum over two separate mechanisms while disregarding the other. Importantly, the frequency up-shift due to the increasing number density, as induced by pair creation, is a much more pronounced effect than the damping [compare Eq. (32)], and this has no correspondence due to radiation reaction. Nevertheless, although

radiation reaction does not change the plasma number density, there will still be a frequency increase due to the decreasing (average) gamma factors, as induced by the energy loss, although that effect is one order higher in α, as compared to the frequency increase due to the Schwinger mechanism.

Finally, it should be noted that there is also a possibility that mechanisms such as Breit-Wheeler pair production could affect the dynamics. In this case, similar dynamics as studied here can be expected, i.e., a frequency up-shift due to the produced pairs; see, e.g., Ref [56]). In the literature, electromagnetic field geometries has often been studied, in which case avalanche processes involving Breit-Wheeler pair production tend to be an important mechanism [9]. However, as indicated by Ref. [10], for a field geometry corresponding to our case, where the particles are accelerated in a given direction, the avalanche processes are not necessarily as strong. In the next section, we will look more closely at the potential contribution of Breit-Wheeler pair production.

VI. NONLINEAR BREIT-WHEELER PAIR PRODUCTION

While we have so far not considered thermal photons, they would be a natural part of a physical system with fermions as described above. Hard photons could also be emitted by the fermions via nonlinear Compton scattering. In this section we will calculate some analytical approximations for nonlinear Breit-Wheeler pair production. While the fields we have consider so far oscillate, we will for simplicity consider an electric field with a single maximum. This should suffice as our main goal here is to find out how the probability scales, rather than finding precise results. Indeed, when the probability for this process is large, i.e., when it is important compared to Schwinger pair production, it would be very difficult to find precise results, because we would need to include higher orders in α, but it is not know how to do that for this type of fields, and the electric field is not a simple background field but determined by back-reaction. So, the best we can do at the moment is to find an estimate for when this becomes important, which we do by considering how many Breit-Wheeler pairs are produced during one (half) cycle. Thus, with these motivating arguments, we consider a general linearly polarized symmetric time-dependent single-pulse field, $A_3(-t) = -A_3(t)$, $A_3(t) = f(\omega t)/\gamma$, where $\gamma = 1/a_0 = \omega/E$ is the Keldysh parameter and a_0 is the classical nonlinearity parameter. (This notation holds for the current section, but differs from previous sections, where we used γ to denote the Lorentz factor.) We expect the process to mainly be a "tunneling" process rather than a multiphoton absorption process. We have performed the calculation using the WKB method as explained in [57], and we refer to that paper for more details. The WKB method for time-dependent electric fields, e.g., rotating, has also been studied recently in [58]. In this section we use units where the electron mass $m = 1$. The initial photon has momentum **k**. We consider an arbitrarily polarized photon, with polarization vector initially described as a superposition of two basis polarization 4-vectors

$$\epsilon_\mu = \cos\left(\frac{\rho}{2}\right)\epsilon_\mu^{(\parallel)} + \sin\left(\frac{\rho}{2}\right)e^{i\lambda}\epsilon_\mu^{(\perp)}, \tag{40}$$

where

$$\epsilon_\mu^{(\parallel)} = \frac{1}{\Omega}\{0, -k_\parallel, 0, k_\perp\} \quad \epsilon_\mu^{(\perp)} = \{0, 0, 1, 0\} \tag{41}$$

for a photon with $k_\mu = \{\Omega, k_\perp, 0, k_\parallel\}$. The polarization vector $\epsilon_\mu^{(\parallel)}$ has a component parallel to the electric field, while $\epsilon_\mu^{(\perp)}$ is perpendicular to both the photon momentum and the field. The probability can be calculated with WKB as explained in [57]. The result is expressed as

$$P = \mathbf{N} \cdot \mathbf{M}, \tag{42}$$

where

$$\mathbf{N} = \{1, \cos\lambda\sin\rho, \sin\lambda\sin\rho, \cos\rho\} \tag{43}$$

is the Stokes vector and we call **M** the Mueller vector (these are not Lorentz 4-vectors). The various integrals are performed using the saddle-point method. For the momentum integrals we have a saddle point where the electron-positron pair share the photon momentum equally, for the canonical momentum of the electron this means $p_\perp = k_\perp/2 = \sqrt{k_1^2 + k_2^2}/2$ and $p_\parallel = k_3/2$, where $\Omega = |\mathbf{k}| = 2\sqrt{p_\perp^2 + p_\parallel^2}$, and $m_\perp = \sqrt{1 + p_\perp^2}$ is an effective mass. We find

$$\mathbf{M} = \frac{\sqrt{\pi}\alpha\omega^{3/2}\{1 + 3p_\perp^2, 0, 0, 1 - p_\perp^2\}}{8\sqrt{2}A'(\tilde{t})\Omega p_\perp m_\perp^2\sqrt{\mathcal{J}_1}}$$

$$\times \left[(\mathcal{J}_1 - p_\perp^2\mathcal{J}_2)m_\perp^2\mathcal{J}_2 - p_\perp^2\mathcal{J}_A^2 \right.$$

$$\left. - \frac{\mathcal{J}_1 - p_\perp^2\mathcal{J}_2 + 2p_\parallel\mathcal{J}_A + \frac{m_\perp^2 p_\parallel^2}{p_\perp^2}\mathcal{J}_2}{1 + \frac{m_\perp^2 p_\parallel^2}{p_\perp^4}} \frac{\omega}{p_\perp A'(\tilde{t})} \right]^{-1/2}$$

$$\times \exp\left[-\frac{4}{\omega}\left(\mathcal{J}_0 - \frac{\Omega\tilde{u}}{2}\right) \right], \tag{44}$$

where the $\mathcal{J}$ functions are given by the following time integrals:

$$\mathcal{J}_n = \frac{1}{2}\int_0^{\tilde{u}} du\left([m_\perp^2 + (A - p_\parallel)^2]^{\frac{1}{2}-n} + [m_\perp^2 + (A + p_\parallel)^2]^{\frac{1}{2}-n}\right), \tag{45}$$

$$\mathcal{J}_A = \frac{1}{2}\int_0^{\tilde{u}} du\left(\frac{A - p_\parallel}{[m_\perp^2 + (A - p_\parallel)^2]^{\frac{3}{2}}} - \frac{A + p_\parallel}{[m_\perp^2 + (A + p_\parallel)^2]^{\frac{3}{2}}}\right), \tag{46}$$

where $u = -i\omega t > 0$ is a rescaled complex time variable, i.e., the integration contour is over a finite interval along the positive imaginary time axis. For the antisymmetric fields we consider, the potential is purely imaginary along this integration contour, so we can write $A(t) = i\tilde{f}(u)/\gamma$, where $\tilde{f}(u)$ is now a real function. The integration limit, $\tilde{u}$, is determined by

$$\tilde{f}(\tilde{u}) = \sqrt{1 + \frac{p_\parallel^2}{p_\perp^2}}\gamma. \tag{47}$$

Note that, in contrast to the perpendicular case ($p_\parallel = 0$) considered in [57], $\tilde{u}$ depends in general on the momentum. Note

that $\mathcal{J}_n$ and $\mathcal{J}_A$ are real. We have

$$\mathcal{J}_1 = \frac{1}{p_\perp} \frac{\partial \mathcal{J}_0}{\partial p_\perp} + \frac{p_\parallel^2}{p_\parallel^3} \frac{\omega}{A'(\tilde{t})}, \tag{48}$$

$$\mathcal{J}_2 = -\frac{1}{p_\perp} \frac{\partial \mathcal{J}_1}{\partial p_\perp} - \frac{p_\parallel^2}{p_\perp(p_\perp^4 + m_\perp^2 p_\parallel^2)} \frac{\omega}{A'(\tilde{t})}, \tag{49}$$

and

$$\mathcal{J}_A = \frac{\partial \mathcal{J}_1}{\partial p_\parallel} - \frac{p_\parallel p_\perp}{p_\perp^4 + m_\perp^2 p_\parallel^2} \frac{\omega}{A'(\tilde{t})}. \tag{50}$$

These relations are very useful in cases where we can calculate $\mathcal{J}_0$ analytically, since then the other integrals are obtained by simply differentiating. In the perpendicular case, $k_\parallel = 0$, we recover immediately the results in [57]. However, to obtain estimates for the present paper, we need to consider photons with $k_\parallel \neq 0$. In fact, most particles have much larger parallel momentum components. As the general result (44) is not particularly illuminating, we will consider various limits.

A. LCF limit

Consider first the locally constant field (LCF) limit, $\gamma \ll 1$. In order to obtain the pre-exponential factor we need to expand the integrals to next-to-leading order, $\mathcal{J} \approx c_1 \gamma + c_3 \gamma^3$. We find

$$\lim_{\gamma \ll 1} \mathbf{M} = \frac{\sqrt{\pi} \alpha E^2(0) \{1 + 3p_\perp^2, 0, 0, 1 - p_\perp^2\}}{8\sqrt{-E''(0)} \Omega p_\perp m_\perp}$$
$$\times \frac{\exp\left\{-\frac{2}{E(0)}[m_\perp^2 \mathrm{arccot}(p_\perp) - p_\perp]\right\}}{\sqrt{\mathrm{arccot}(p_\perp)}[m_\perp^2 \mathrm{arccot}(p_\perp) - p_\perp]}, \tag{51}$$

where we have assumed that the field has a maximum at $t = 0$. This agrees with what one finds by starting with Eq. (6) in [59] for nonlinear Breit-Wheeler in a constant electric field, replacing the volume factor by a time integral, $V_0 \to \int dt$, and the constant field with a locally constant field, $E \to E(t)$, and then performing this time integral with the saddle-point method. This prescription for how to go from a constant-field result to a LCF approximation has been applied to Schwinger pair production in [60]. Note that in this limit the result only depends on $p_\parallel$ via Ω. We have $E''(0) = E\omega^2 f'''(0)$, where $f'''(0) = d_u^3 f(u)|_{u=0}$ is $O(1)$ [e.g., $f'''(0) = -2$ for a Sauter pulse, $f(u) = \tanh(u)$]. Hence, with $E = E(0)$ and $\gamma = \omega/E = 1/a_0$ as independent parameters, the probability scales as

$$P = \alpha \mathcal{A} \sqrt{E} F(p_\perp) e^{-G(p_\perp)/E}, \tag{52}$$

where

$$\mathcal{A} = \frac{k_\perp}{\sqrt{k_\perp^2 + k_\parallel^2}} a_0. \tag{53}$$

We will argue that $\mathcal{A}$ is an important parameter for estimating the size of the probability. This can also be expressed as (compare with the case of null fields [61])

$$\mathcal{A} = \frac{\chi}{b_0}, \tag{54}$$

where $\chi = \sqrt{-(F^{\mu\nu}k_\nu)^2}$ and $b_0 = \kappa k$, where $\kappa = \{\omega, 0, 0, 0\}$ is the wave vector of the field. The fact that $\mathcal{A}$ is a relevant parameter beyond the LCF limit considered in this subsection can already be seen by noting that (47) can be expressed as

$$\tilde{f}(\tilde{u}) = \frac{1}{\mathcal{A}}. \tag{55}$$

Although one can only expect the saddle-point approximation to be precise for sufficiently small E, one can expect it to still give an order of magnitude estimate for $E \lesssim 1$. So, if $k_\perp, k_\parallel \sim 1$ and a_0 is sufficiently large then we could have $\alpha a_0 \sim 1$, which would make the probability large, which in turn would mean that we would need to take higher orders in α into account. However, in the system that we have focused on above, the fermions typically have momenta that are almost parallel to the field, i.e., $p_\parallel \gg p_\perp$. We can use the Lorentz-force equation to estimate $p_\parallel \sim a_0$ as a typical momentum. If the photon considered in this section has been emitted by such a fermion, we also expect the photon to have a momentum almost parallel to the field. For $k_\parallel = 2p_\parallel \sim a_0$ and $k_\perp \sim 1$ we have

$$\mathcal{A} \sim \frac{a_0}{k_\parallel} \sim 1, \tag{56}$$

which is not large, and then there is no large factor to compensate for $\alpha \ll 1$ in (52). Thus, for the system we consider, where the particles tend to have large parallel momentum, the Breit-Wheeler process would be less important. However, as (51) has been derived with $\gamma \ll 1$ as expansion parameter, i.e., implicitly assuming that no other parameter is too small or large, we will derive a new result specifically for the limit $p_\parallel \sim a_0 \gg 1$ in order to confirm this. But first we consider another limit which allows us to make another nontrivial check of (44).

B. Plane-wave limit

Next we consider the limit where both the perpendicular and the parallel momentum components are large, or where only the perpendicular component is large. We find

$$\lim_{p_\perp \sim p_\parallel \gg 1} \mathbf{M} = \frac{\alpha \sqrt{\pi} \chi \{3, 0, 0, -1\} \exp\left\{-\frac{4\mathcal{A}}{\chi}(\tilde{u} - \mathcal{A}^2 \mathcal{J}_{\mathrm{PW}})\right\}}{32\mathcal{A}\sqrt{\tilde{u}\tilde{f}'(\tilde{u})(\tilde{u} - \mathcal{A}^2 \mathcal{J}_{\mathrm{PW}})(\mathcal{A}\tilde{u}\tilde{f}'(\tilde{u}) - 1)}}, \tag{57}$$

where $\chi = \sqrt{-(F^{\mu\nu}k_\nu)^2} = Ek_\perp = 2Ep_\perp$ and

$$\mathcal{J}_{\mathrm{PW}} = \int_0^{\tilde{u}} du \tilde{f}^2(u). \tag{58}$$

Thus,

$$P = \alpha \sqrt{\chi} F_{\mathrm{PW}}(\mathcal{A}) e^{-G_{\mathrm{PW}}(\mathcal{A})/\chi}. \tag{59}$$

This agrees with the result for nonlinear Breit-Wheeler in a plane wave instead of $E(t)$ [see Eq. (166) in [57]] but with $\mathcal{A}$ instead of just a_0. Thus, we again see that it is $\mathcal{A}$ rather than just a_0 that is the relevant parameter.

One can understand this using a Lorentz boost as follows. In terms of the two orthonormal vectors $\hat{\mathbf{k}} = \mathbf{k}/|\mathbf{k}|$ and $\boldsymbol{\epsilon}_\parallel$ (the spatial components of $\epsilon_\mu^{(\parallel)}$) the electric field can be

expressed as

$$\mathbf{E}(t) = \frac{1}{\Omega}(k_\parallel \hat{\mathbf{k}} + k_\perp \boldsymbol{\epsilon}_\parallel)E(t), \tag{60}$$

so the field components parallel and perpendicular to the photon momentum are given by

$$E_\parallel = \frac{k_\parallel}{\Omega}E \quad E_\perp = \frac{k_\perp}{\Omega}E. \tag{61}$$

Note that, e.g., $k_\parallel$ gives the momentum component parallel to the electric field, while $E_\parallel$ gives the component of the electric field that is parallel to the photon momentum. In order to get rid of the large parameter, we boost along the photon momentum to a frame where the photon momentum is [63] $O(1)$. In this new frame the perpendicular components of the field are given by

$$E'_\perp = \gamma_L E_\perp \quad \mathbf{B}'_\perp \approx -\gamma_L \hat{\mathbf{k}} \times \mathbf{E}_\perp, \tag{62}$$

where $\gamma_L = 1/\sqrt{1 - v^2}$ is the Lorentz factor of the boost, while the parallel components remain the same, $E'_\parallel = E_\parallel$ and $B'_\parallel = 0$. Since we need to boost with a speed v close to the speed of light, $\gamma_L \gg 1$, and hence the perpendicular components are much larger than the parallel components, and the field in the new frame is approximately null, $\mathbf{E}'^2 - \mathbf{B}'^2 \approx \mathbf{E}' \cdot \mathbf{B}' \approx 0$. Moreover, in this new frame the argument of the field is approximately lightlike,

$$\omega t \rightarrow \gamma_L \omega(t' + \hat{\mathbf{k}} \cdot \mathbf{x}') = \omega'(t' + \hat{\mathbf{k}} \cdot \mathbf{x}'). \tag{63}$$

Thus, in the new frame the field is basically a plane wave, and the corresponding "classical nonlinearity parameter" is the ratio of the field strength and frequency in this frame,

$$a'_0 := \frac{E'}{\omega'} = \frac{E_\perp}{\omega} = \frac{k_\perp}{\sqrt{k_\perp^2 + k_\parallel^2}}a_0 = \mathcal{A}. \tag{64}$$

Thus, this Lorentz transformation shows that when we have a large perpendicular momentum we expect the probability to be approximately equal to the corresponding result for Breit-Wheeler in a plane wave with classical nonlinearly parameter given by $\mathcal{A}$, and this is indeed what we found in (57). Since (57) has the same functional form as for a plane wave, we already know from the literature its various limits and special cases. For large $\mathcal{A}$, (57) reduces to

$$\lim_{\mathcal{A} \gg 1} \lim_{p_\perp \sim p_\parallel \gg 1} \mathbf{M} = \frac{3\alpha \mathcal{A}\sqrt{\pi \chi}f'(0)^2\{3, 0, 0, -1\}}{32\sqrt{-2f'''(0)}}e^{-\frac{8}{3\chi f'(0)}}, \tag{65}$$

which agrees with the LCF approximation that one can obtain by starting with results for a constant-crossed field [64–66]. We again see that a large $\mathcal{A}$ can compensate for $\alpha \ll 1$, but a large a_0 may not be enough if $k_\parallel \gg k_\perp$.

C. Large longitudinal limit

Now we return to the limit that is most relevant for the previous sections, i.e., where $a_0 \gg 1$ and where the particles have a large longitudinal momentum because they have been accelerated by the field, or because they have been produced by particles with such a momentum. If the momentum is

mostly due to the Lorentz force then we have

$$P_\parallel \sim E\,\Delta t \sim \frac{E}{\omega} = a_0, \tag{66}$$

where we have used $1/\omega$ as a typical timescale. At least in the saddle-point regime, we expect the produced fermions in trident to have momentum on the same order of magnitude as the initial electron's momentum, which also means that the intermediate photon has a similar momentum scale. It is therefore justified to consider nonlinear Breit-Wheeler for a photon with momentum $k_\parallel \sim a_0$. We find

$$\lim_{p_\parallel \sim a_0 \gg 1} \mathbf{M} = \frac{\alpha \sqrt{\pi E}\{1 + 3p_\perp^2, 0, 0, 1 - p_\perp^2\}}{16\sqrt{2}p_\perp m_\perp \tilde{f}'(\tilde{u})\sqrt{\mathcal{S}_1}}$$

$$\times \left[\hat{p}_\parallel^2 m_\perp^2\big(m_\perp^2 \mathcal{S}_1 \mathcal{S}_2 - p_\perp^2 \mathcal{S}_A^2\big) \right.$$

$$\left. - (\hat{p}_\parallel^2 m_\perp^2 \mathcal{S}_2 + p_\perp^2[\mathcal{S}_1 + 2\hat{p}_\parallel \mathcal{S}_A])\frac{p_\perp}{\tilde{f}'(\tilde{u})} \right]^{-\frac{1}{2}}$$

$$\times \exp\left[-\frac{2}{E}\left(m_\perp^2 \mathcal{S}_1 - \frac{p_\perp^2}{\hat{p}_\parallel}\tilde{u}\right) \right], \tag{67}$$

where $\hat{p}_\parallel = p_\parallel/a_0 \sim O(1)$, $\tilde{f}(\tilde{u}) = \hat{p}_\parallel/p_\perp$,

$$\mathcal{S}_1 = \int_0^{\tilde{u}} du \frac{\hat{p}_\parallel}{\hat{p}_\parallel^2 + \tilde{f}^2(u)}, \tag{68}$$

$$\mathcal{S}_2 = \int_0^{\tilde{u}} du \frac{\hat{p}_\parallel[\hat{p}_\parallel^2 - 3\tilde{f}^2(u)]}{[\hat{p}_\parallel^2 + \tilde{f}^2(u)]^3}, \tag{69}$$

and

$$\mathcal{S}_A = \int_0^{\tilde{u}} du \frac{\tilde{f}^2(u) - \hat{p}_\parallel^2}{[\hat{p}_\parallel^2 + \tilde{f}^2(u)]^2}. \tag{70}$$

Although this looks more complicated compared to the other limits, we can immediately see that (67) is independent of a_0 [with $\hat{p}_\parallel$ as an independent $O(1)$ parameter], and the probability scales as

$$P = \alpha\sqrt{E}F_{\text{long}}(p_\perp, \hat{p}_\parallel)e^{-G_{\text{long}}(p_\perp, \hat{p}_\parallel)/E}. \tag{71}$$

This agrees with what we found by taking the large $p_\parallel$ limit of the LCF or plane-wave limits. Thus, this confirms the tentative conclusions made in the previous subsections. In particular, there is no large parameter in this limit to compensate for $\alpha \ll 1$, and so the Breit-Wheeler probability is suppressed by a factor of α.

We can understand these results using a Lorentz boost similar to the plane-wave case. However, in this case we should boost parallel to the electric field in order to reduce the large longitudinal momentum to $p'_\parallel \sim O(1)$. For such a boost there is no change in the direction or strength of the electric field and there is no induced magnetic field. The only change on the field is that the argument becomes lightlike

$$\omega t \rightarrow \gamma_L \omega(t' \pm z') = \omega'(t' \pm z'). \tag{72}$$

Thus, in the new frame we have a field on the form $E_{z'}(t' + z')$. Schwinger pair production in such a field has been studied in

[67,68]. We can define a classical nonlinearity parameter in the new frame as

$$a'_0 := \frac{E'}{\omega'} = \frac{a_0}{\gamma_L}. \tag{73}$$

But in order for $k'_\parallel \sim O(1)$ we need $\gamma_L \sim k_\parallel \sim a_0$, which means $a'_0 \sim O(1)$. Thus, this Lorentz boost does two things: it makes $k'_\mu \sim O(1)$ and gives a $a'_0 \sim O(1)$. Since $\mathcal{A} \sim 1$ too, using $\mathcal{A}$ as a more general nonlinearity parameter also works in this limit. There is therefore no large factor that can compensate for $\alpha \ll 1$. Note that this Lorentz-boost argument does not rely on the saddle-point approximation, so we might expect that the same argument would imply that the probability is relatively small in a larger parameter regime.

In this section we have considered nonlinear Breit-Wheeler pair production. Another process that would be directly relevant to check as a competing process is the nonlinear trident process, $e^- \to e^- e^- e^+$. It is possible to derive similar results for this process, but the results will be presented elsewhere. However, the main message about how the probability scales is similar. Indeed, we can use the same Lorentz-transformation arguments as above. Thus, it is again $\mathcal{A}$ that is the relevant parameter (defined with the initial electron momentum). For large $\mathcal{A}$, trident at $O(\alpha^2)$ would to leading order scale as $(\alpha \mathcal{A})^2$. If this is not small then one would need to include higher orders, but it tends to be small for the system we have considered here.

VII. CONCLUSION

The main purpose of this study has been to study self-consistent plasma dynamics for ultrastrong field strengths. It is seen that for fields strengths of the order E_{cr} or larger, electron-positron pair production leads to a pronounced increase in the plasma oscillation frequency, and also damping of the amplitude. The scaling of the damping with the plasma parameters has been investigated numerically. In particular, for a fixed chemical potential μ, pair production is suppressed for higher temperatures. This is because the mechanism depends sensitively on the plasma density, which is increased with higher temperature (for a fixed μ). However, if the particle number density is kept fixed instead, there is a slight increase in the damping with temperature. This is because more low-energy states will be available for pair creation.

For numerical convenience, we have picked fairly high plasma densities in our study, since the code can be executed on a PC in this case. However, from the point of view of laboratory experiments, the case with μ and T much less than unity is of most interest. While we have not probed this regime here, the scaling behavior displayed in Fig. 6 still applies. Nevertheless, extended simulations (run on a parallel computer) must be made for detailed quantitative predictions in the regime where both $\mu \ll 1$ and $T \ll 1$ applies.

For field strength well beyond E_{cr}, the dynamics is similar to the case $E \sim E_{cr}$, but the processes is considerably more rapid. Moreover, starting with an electron-positron plasma as initial condition, the process can evolve in the opposite direction. That is, instead of Schwinger pair production, we can have collective Schwinger annihilation, leading to an increase in the oscillation amplitude. While this process is much faster than collisional annihilation, it still competes with pair production taking place in the part of momentum space that is not filled with electrons and positrons. Thus, as far as we have seen, pair annihilation is typically not a dominant mechanism.

For strong fields, certain processes not covered by the DHW formalism are potentially important. This includes radiation reaction and nonlinear Breit-Wheeler pair production. While these processes tend to be important for electromagnetic field geometry, the estimates given in Secs. V and VI indicate that there is a regime of self-consistent dynamics where the Schwinger mechanism is the main feature. In particular, this holds for electric fields of the order of the Schwinger critical field (or somewhat larger), and for a field geometry where the particle momentum is mainly parallel to the electric field.

In conclusion, the DHW formalism is very well suited for studies of collective strong field plasma dynamics. Future problems of interest based on this approach include extensions to nonhomogeneous systems, electromagnetic fields [45,69], and magnetized plasmas.

ACKNOWLEDGMENT

[1] A. Di Piazza, C. Müller, K. Z. Hatsagortsyan, and C. H. Keitel, Rev. Mod. Phys. **84**, 1177 (2012).

[2] A. Fedotov, A. Ilderton, F. Karbstein, B. King, D. Seipt, H. Taya, and G. Torgrimsson, Phys. Rep. **1010**, 1 (2023).

[3] http://www.extreme-light-infrastructure.eu/

[4] J. Schwinger, Phys. Rev. **82**, 664 (1951).

[5] A. I. Nikishov, JETP **30**, 660 (1970).

[6] T. D. Cohen and D. A. McGady, Phys. Rev. D **78**, 036008 (2008).

[7] S. P. Kim and D. N. Page, Phys. Rev. D **73**, 065020 (2006).

[8] F. Quéré and H. Vincenti, HPLSE **9**, 6 (2021).

[9] A. M. Fedotov, N. B. Narozhny, G. Mourou, and G. Korn, Phys. Rev. Lett. **105**, 080402 (2010).

[10] S. S. Bulanov, T. Zh. Esirkepov, A. G. R. Thomas, J. K. Koga, and S. V. Bulanov, Phys. Rev. Lett. **105**, 220407 (2010).

[11] E. S. Efimenko, A. V. Bashinov, A. A. Gonoskov, S. I. Bastrakov, A. A. Muraviev, I. B. Meyerov, A. V. Kim, and A. M. Sergeev, Phys. Rev. E **99**, 031201(R) (2019).

[12] F. Hebenstreit, R. Alkofer, and H. Gies, Phys. Rev. D **82**, 105026 (2010).

[13] F. Hebenstreit, R. Alkofer, and H. Gies, Phys. Rev. Lett. **107**, 180403 (2011).

[14] I. A. Aleksandrov and C. Kohlfürst, Phys. Rev. D **101**, 096009 (2020).

[15] C. Kohlfürst, Phys. Rev. D **101**, 096003 (2020).

[16] A. Gonoskov, I. Gonoskov, C. Harvey, A. Ilderton, A. Kim, M. Marklund, G. Mourou, and A. Sergeev, Phys. Rev. Lett. **111**, 060404 (2013).

[17] S. S. Bulanov, V. D. Mur, N. B. Narozhny, J. Nees, and V. S. Popov, Phys. Rev. Lett. **104**, 220404 (2010).

[18] F. Cooper and E. Mottola, Phys. Rev. D **40**, 456 (1989).

[19] Y. Kluger, J. M. Eisenberg, B. Svetitsky, F. Cooper, and E. Mottola, Phys. Rev. D **45**, 4659 (1992).

[20] R. Ruffini, L. Vitagliano, and S. S. Xue, Phys. Lett. B **559**, 12 (2003).

[21] J. C. R. Bloch, V. A. Mizerny, A. V. Prozorkevich, C. D. Roberts, S. M. Schmidt, S. A. Smolyansky, and D. V. Vinnik, Phys. Rev. D **60**, 116011 (1999).

[22] F. Hebenstreit, J. Berges, and D. Gelfand, Phys. Rev. D **87**, 105006 (2013).

[23] A. Otto, D. Graeveling, and B. Kämpfer, Plasma Phys. Control. Fusion **61**, 074002 (2019).

[24] G. Gold, D. A. Mcgady, S. P. Patil, and V. Vardanyan, J. High Energy Phys. 10 (2021) 072.

[25] B. Buyens, J. Haegeman, F. Hebenstreit, F. Verstraete, and K. Van Acoleyen, Phys. Rev. D **96**, 114501 (2017).

[26] V. Kasper, F. Hebenstreit, and J. Berges, Phys. Rev. D **90**, 025016 (2014).

[27] V. Kasper, F. Hebenstreit, F. Jendrzejewski, M. K. Oberthaler, and J. Berges, New J. Phys. **19**, 023030 (2017).

[28] V. Kasper, F. Hebenstreit, M. Oberthaler, and J. Berges, Phys. Lett. B **760**, 742 (2016).

[29] F. Gelis and N. Tanji, Phys. Rev. D **87**, 125035 (2013).

[30] F. Gelis and N. Tanji, Prog. Part. Nucl. Phys. **87**, 1 (2016).

[31] N. Tanji, Ann. Phys. **324**, 1691 (2009).

[32] F. Sauter, Z. Phys. **69**, 742 (1931).

[33] I. Bialynicki-Birula, P. Gornicki, and J. Rafelski, Phys. Rev. D **44**, 1825 (1991).

[34] H. Al-Naseri and G. Brodin, Phys. Plasmas **29**, 042106 (2022).

[35] H. Al-Naseri, J. Zamanian, and G. Brodin, Phys. Rev. E **104**, 015207 (2021).

[36] G. Fauth, J. Berges, and A. Di Piazza, Phys. Rev. D **104**, 036007 (2021).

[37] D. Vasak, M. Gyulassy, and H. T. Elze, Ann. Phys. **173**, 462 (1987).

[38] X. L. Sheng, R. H. Fang, Q. Wang, and D. H. Rischke, Phys. Rev. D **99**, 056004 (2019).

[39] We will refer to the given field as electrostatic, since there is no magnetic field. However, aiming for an electrostatic scalar potential in the homogeneous limit is not possible, as the scalar potential would then be infinite. Sometimes the field used here is seen as the dipole approximation of an electromagnetic field. The possibility to use opposing terminology for the same physical setup appears because the electrostatic Langmuir wave and the electromagnetic wave coincides in the limit of infinite wavelength.

[40] G. Brodin and J. Zamanian, Rev. Mod. Plasma Phys. **6**, 4 (2022).

[41] W. H. Press, S. A. Teukolsky, W. T. Vetterling, and B. P. Flannery, *Numerical Recipes 3rd Edition: The Art of Scientific Computing* (Cambridge University Press, Cambridge, 2007).

[42] S. P. Gavrilov and D. M. Gitman, Phys. Rev. Lett. **101**, 130403 (2008).

[43] S. P. Gavrilov and D. M. Gitman, Phys. Rev. D **78**, 045017 (2008).

[44] K. Krajewska and J. Z. Kaminski, Phys. Rev. A **100**, 012104 (2019).

[45] S. S. Bulanov, A. M. Fedotov, and F. Pegoraro, Phys. Rev. E **71**, 016404 (2005).

[46] Note that in the presence of an external Sauter pulse, in order for the electric field to obey Maxwell's equation (in particular fulfill Ampère's law), we must formally assume the presence of an external current that is the source of the pulse. Such a current should then be added to the self-consistent plasma current in Eq. (12).

[47] A. Gonoskov, S. Bastrakov, E. Efimenko, A. Ilderton, M. Marklund, I. Meyerov, A. Muraviev, A. Sergeev, I. Surmin, and E. Wallin, Phys. Rev. E **92**, 023305 (2015).

[48] M. Marklund, B. Eliasson, P. K. Shukla, L. Stenflo, M. E. Dieckmann, and M. Parviainen, JETP Lett. **83**, 313 (2006).

[49] A. Rohatgi, WebPlotDigitizer, https://apps.automeris.io/wpd/

[50] L. D. Landau and E. M. Lifshitz, *The Classical Theory of Fields* (Pergamon Press, Oxford, 1975).

[51] A. I. Nikishov and V. I. Ritus, Zh. eksper. teor. fiz. **46**, 776 (1963) [Sov. Phys. JETP 19, 529 (1964)].

[52] V. B. Berestetskii, E. M. Lifshits, and L. P. Pitaevskii, *Quantum Electrodynamics* (Pergamon Press, New York, 1982).

[53] Another way of obtaining this is from the Larmor formula, $P(p) = -(2/3)e^2 \dot{p}_\mu^2$, by approximating $P(p_{RR}) \approx P(p_{Lo})$, where p_{Lo}^μ is the solution to the Lorentz force equation without RR, $\dot{p}^\mu = eF^{\mu\nu}p_\nu/m$.

[54] A. Gonoskov, T. G. Blackburn, M. Marklund, and S. S. Bulanov, Rev. Mod. Phys. **94**, 045001 (2022).

[55] D. Seipt, T. Heinzl, M. Marklund, and S. S. Bulanov, Phys. Rev. Lett. **118**, 154803 (2017).

[56] K. Qu, S. Meuren, and N. J. Fisch, Phys. Rev. Lett. **127**, 095001 (2021).

[57] G. Degli Esposti and G. Torgrimsson, Phys. Rev. D **105**, 096036 (2022)

[58] E. G. Gelfer, A. M. Fedotov, A. A. Mironov, and S. Weber, Phys. Rev. D **106**, 056013 (2022).

[59] G. V. Dunne, H. Gies, and R. Schutzhold, Phys. Rev. D **80**, 111301(R) (2009).

[60] G. V. Dunne, Q. h. Wang, H. Gies, and C. Schubert, Phys. Rev. D **73**, 065028 (2006).

[61] In this form it resembles the manifestly Lorentz and gauge invariant representation of a_0 given in [62] for null fields, i.e. fields with $\mathbf{E}^2 - \mathbf{B}^2 = \mathbf{E} \cdot \mathbf{B} = 0$. If the combination χ/b_0 is evaluated for plane waves, which are the most common null fields, then one finds $\chi/b_0 = a_0 = E/\omega$. The fields we consider, on the other hand, are not null nor approximately null, but we find that χ/b_0 is still a relevant parameter. We have chosen to denote this as $\mathcal{A} := \chi/b_0 \neq E/\omega =: a_0$.

[62] T. Heinzl and A. Ilderton, Opt. Commun. **282**, 1879 (2009).

[63] When the same argument is used for a process with a single fermion in the initial state, it would be possible to go to its rest frame, but that is not actually relevant for this argument. We only need to go to a frame where the momentum is of the order of the electron mass.

[64] V. I. Ritus, J. Russ. Laser Res. **6**, 497 (1985).

[65] H. R. Reiss, J. Math. Phys. **3**, 59 (1962).

[66] A. I. Nikishov and V. I. Ritus, JETP **19**, 529 (1964).

[67] T. N. Tomaras, N. C. Tsamis, and R. P. Woodard, J. High Energy Phys. 11 (2001) 008.

[68] A. Ilderton, J. High Energy Phys. 09 (2014) 166.

[69] N. Mueller, F. Hebenstreit, and J. Berges, Phys. Rev. Lett. **117**, 061601 (2016).